

RESEARCH ARTICLE | AUGUST 04 2005

Monte Carlo simulations of hydrogen adsorption in alkali-doped single-walled carbon nanotubes

Naiping Hu; Xiaoyang Sun; Andrew Hsu




J. Chem. Phys. 123, 044708 (2005)

<https://doi.org/10.1063/1.1954727>




CrossMark



The Journal of Chemical Physics

Special Topic: Algorithms and Software
for Open Quantum System Dynamics

Submit Today



Monte Carlo simulations of hydrogen adsorption in alkali-doped single-walled carbon nanotubes

Naiping Hu, Xiaoyang Sun, and Andrew Hsu^{a)}

Department of Mechanical Engineering, Indiana University–Purdue University Indianapolis, Indianapolis, Indiana 46202

(Received 8 December 2004; accepted 23 May 2005; published online 4 August 2005)

Monte Carlo simulations and Widom's test particle insertion method have been used to calculate the solubility coefficients (S) and the adsorption equilibrium constants (K) in single-walled (10,10) armchair carbon nanotubes including single nanotubes, and nanotube bundles with various configurations with and without alkali dopants. The hydrogen adsorption isotherms at room temperature were predicted by following the Langmuir adsorption model using the calculated constants S and K . The simulation results were in good agreement with experimental data as well as the grand canonical Monte Carlo simulation results reported in the literature. The simulations of nanotube bundle configurations suggest that the gravimetric hydrogen adsorption increases with internanotube gap size. It may be attributed to favorable hydrogen-nanotube interactions outside the nanotubes. The effect of alkali doping on hydrogen adsorption was studied by incorporating K^+ or Li^+ ions into nanotube arrays using a Monte Carlo simulation. The results on hydrogen adsorption isotherms indicate hydrogen adsorption of 3.95 wt% for K-doping, and 4.21 wt% for Li-doping, in reasonable agreement with the experimental results obtained at 100 atm and room temperature.

© 2005 American Institute of Physics. [DOI: 10.1063/1.1954727]

INTRODUCTION

Carbon nanotubes consist of a graphite sheet rolled up into a cylinder of a few nanometers in diameter and several microns in length. Since their discovery in 1991 by Iijima as nested structures of concentric shells,¹ carbon multiwall and single-wall nanotubes (SWNTs) have been synthesized using carbon-arc vaporization,² catalytic decomposition of organic vapors,³ or laser vaporization,⁴ and have been shown to possess potential as a stable and effective adsorbent material for hydrogen storage. Nanotubes have large theoretical surface areas similar to that of high-surface area activated carbons.⁵ In addition, the capillary forces in the micropores of nanotubes can encapsulate both polar and nonpolar fluids.^{6,7} In a first experiment by Dillon *et al.*,⁸ hydrogen adsorption in nanotubes at standard ambient conditions was estimated to be between 5–10 wt% on early SWNT materials. Higher hydrogen adsorptions were reported experimentally on purified crystalline ropes of SWNTs,⁹ arc-generated and purified SWNTs,¹⁰ and multiwalled carbon nanotubes (MWNTs).¹¹ While the results are encouraging, they do not meet the DOE targets of 6.5 wt% and 62 kg H_2/m^3 for hydrogen storage. In 1999, Chen *et al.*¹² reported 20 wt% and 14 wt% of hydrogen adsorption on lithium-doped and potassium-doped MWNTs, respectively. Later Yang¹³ prepared the doped nanotubes following a procedure similar to that of Chen *et al.* but obtained a dry hydrogen adsorption of 2.5 wt% and 1.5 wt% in alkali-doped nanotubes. Pinkerton *et al.* reported results similar to Yang's on lithium-doped nanotubes.¹⁴

In order to understand the hydrogen adsorption process

and the effect of nanotube configurations on hydrogen adsorption, several researchers used Monte Carlo simulations in grand canonical ensembles to predict hydrogen adsorption isotherms in nanotubes.^{5,15–19} The influence of the pore size and geometry as well as the pressure and temperature was reported in these studies.^{5,15} The agreement between these simulations and the experimental results indicates that the atoms in carbon nanotubes and their interaction with other particles can be accurately described with existing potential functions used for planar graphite surface simulations.²⁰

In the present paper we suggest a simple method for the prediction of SWNT hydrogen adsorption isotherms. In this procedure, the excess chemical potential (μ_{ex}) and solubility coefficient (S) are directly calculated using a Widom test particle insertion method,²¹ and the isotherms are then obtained following the Langmuir adsorption model.²² The Widom test particle insertion method was developed by Widom in the 1960s and has been used in the simulations of phase equilibrium²³ and gas solubilities in hydrocarbons,²⁴ ionic liquids,²⁵ and polymers.^{26,27} The objectives of the present study are to calculate the solubility coefficients of hydrogen in SWNTs and alkali-doped SWNTs using this Monte Carlo approach and to study the effect of alkali doping on the hydrogen adsorption process.

COMPUTATIONAL METHODOLOGY

Widom's test particle insertion method

A simple NVT Monte Carlo simulation using Widom's test particle insertion scheme was implemented to calculate the excess chemical potential and solubility coefficient of hydrogen adsorption in carbon nanotubes. Widom's test par-

^{a)}Author to whom correspondence should be addressed. Electronic mail: anhsu@iupui.edu

TABLE I. L-J potential parameters.

Atom i	A_i	B_i	ϵ/k (K)	σ (Å)
C	7108.4660	32.8708	74.78	3.62
H	2 968 753.3590	1325.7081	18.3	2.46
Li	5 192 358.66	9916.8177	2392.64	2.84
K	24 856 948.1942	23 280.4832	2754.44	3.20

ticle insertion method employs a penetrant molecule inserted at a random position and orientation into the fluid. The random insertion is repeated many times on many different configurations and the excess chemical potential is calculated from the following expression:

$$\mu_{ex} = -kT \ln \left\langle \exp \left(-\frac{\Psi}{kT} \right) \right\rangle, \quad (1)$$

where k is the Boltzmann's constant, Ψ is the potential energy change introduced by a particle insertion, T is the temperature, and $\langle \exp(-\Psi/(kT)) \rangle$ is the canonical average of interaction energy; the solubility coefficient can be calculated from the excess chemical potential as follows:

$$S = \exp \left(-\frac{\mu_{ex}}{RT} \right). \quad (2)$$

The iteration number and grid spacing used in the Monte Carlo and Widom's test particle insertion methods are important simulation parameters. The iteration number is the total number of hydrogen insertions used to calculate the ensemble average. An optimal iteration number can yield a higher accuracy of the ensemble average as well as save computation time. Grid spacing is the mesh grid length used to divide the nanotube volume for hydrogen insertion. Accurate simulation results can be obtained using very fine grid spacing but it would be very time-consuming. The selection of iteration number and grid spacing for simulations in this study will be discussed later.

Potential interactions

Molecular interaction energy between two nonbonded atoms i and j can be described by the Lennard-Jones (L-J) potential model as follows:

$$E_k = \frac{A_{ij}}{r^{12}} - \frac{B_{ij}}{r^6}, \quad (3)$$

where A_{ij} , B_{ij} can be given by a geometric mixing rule

TABLE II. Comparison of Lennard-Jones potential parameters.

L-J parameters	ϵ/k (K)	σ (Å)	Reference
Hydrogen-hydrogen	33.3	2.97	17
	36.7	2.96	Present and 18–20
	12.5	2.59	29
	18.3	2.46	CVFF, present and 30
Carbon-hydrogen	30.5	3.19	17
	32.2	3.18	Present and 18–20
	18.7	2.99	29
	26.1	2.98	CVFF, present and 30

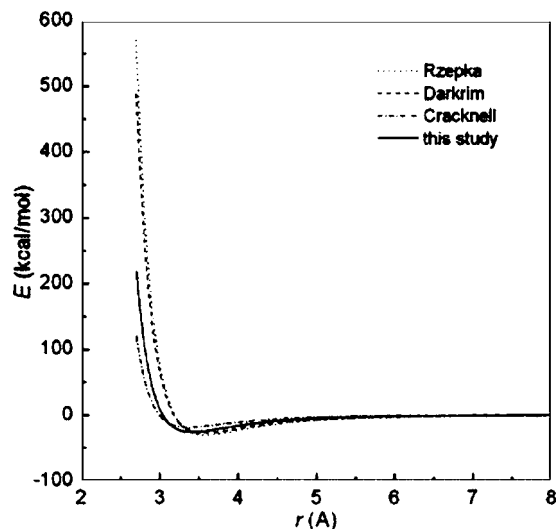


FIG. 1. Comparison of force field parameters used by various authors.

$$A_{ij} = \sqrt{A_i A_j} \quad \text{and} \quad B_{ij} = \sqrt{B_i B_j} \quad (4)$$

where A_i, B_i and A_j, B_j are Lennard-Jones constants for atom types i and j , respectively. A completely equivalent representation is

$$E_{ij} = 4\epsilon_{ij} \left[\left(\frac{\sigma_{ij}}{r} \right)^{12} - \left(\frac{\sigma_{ij}}{r} \right)^6 \right], \quad (5)$$

where ϵ_{ij} is the potential well depth in kcal mol⁻¹ and σ_{ij} is the interatomic distance at which a zero potential energy occurs. The conversion between the two representations (4) and (5) is straightforward:

$$A_{ij} = 4\epsilon_{ij}\sigma_{ij}^{12}, \quad (6)$$

$$B_{ij} = 4\epsilon_{ij}\sigma_{ij}^6.$$

The L-J potential parameters used in this study are taken from the CVFF force field²⁸ (Table I), which was shown to

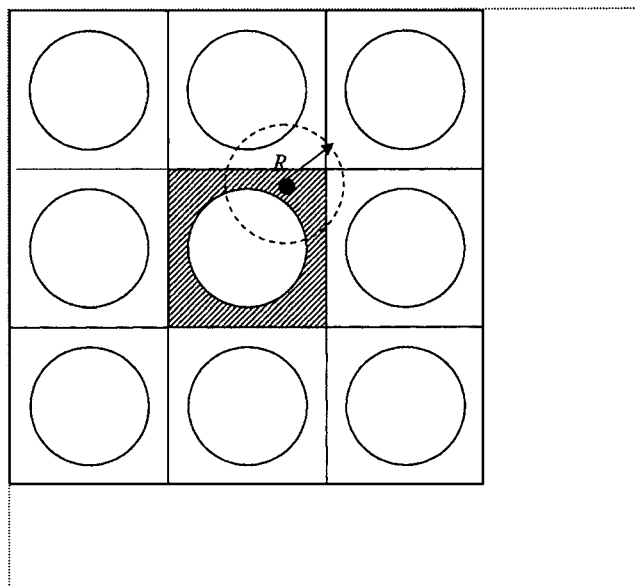


FIG. 2. Periodic boundary condition and cutoff radius used in the simulations. ● indicates the position of a hydrogen test molecule.

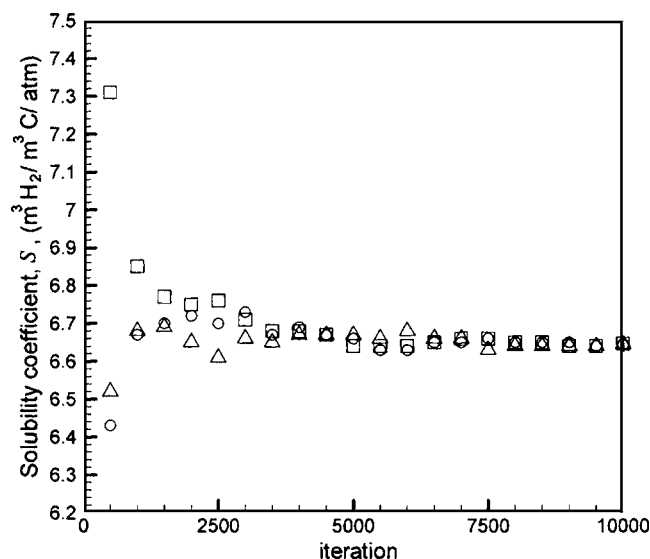


FIG. 3. Representative convergence plots obtained from Widom's test particle insertion simulations over 10 000 iteration steps.

work well for hydrogen storage in nanotubes in a study by Dodziuk and Dolgonos.²⁹ The CVFF parameters are compared with the parameters used in other carbon nanotube and hydrogen storage studies^{17–20,30} in Table II and Fig. 1. As shown, the L-J parameters for carbon-hydrogen and hydrogen-hydrogen interactions used in this study are comparable to the force field parameters well tested and validated in other studies. To verify that the minor differences in force field parameters will not result in appreciable differences in the predicted results, the well tested force field parameters used in Refs. 18–20 are also employed in the present study and the results are compared, in the Results and Discussion section, with those obtained using the CVFF force field.

The electronic interactions between two dopant ions, E^{ele1} , and the charge-hydrogen interactions between a dopant ion and a hydrogen molecule, E^{ele2} , are calculated using the long-range Coulombic potential and the charge-quadrupole potential, respectively,

$$E_{i,j}^{\text{ele1}} = \frac{1}{4\pi\epsilon_0} \frac{q_i q_j}{r}, \quad (7)$$

$$E_{i,j}^{\text{ele2}} = \frac{1}{8\pi\epsilon_0} \frac{q_i \Theta_j}{r^3} (3 \cos^2(\phi) - 1),$$

where q_i, q_j are the formal charges of ions i and j , Θ_j is the quadrupole moment of the hydrogen molecule [0.9203 a.u. (Ref. 31)], ϕ is the angle that indicates the orientation between the hydrogen molecule and a carbon atom, and ϵ_0 is the electrical permittivity of space. However, both E^{ele1} and E^{ele2} are negligibly small for all values of the distance, r , compared to the Lennard-Jones potential calculated from the CVFF force field parameters.

Periodic boundary condition and cutoff radius for potential

A periodic boundary condition was applied in the simulations of single nanotube and nanotube bundles. Figure 2

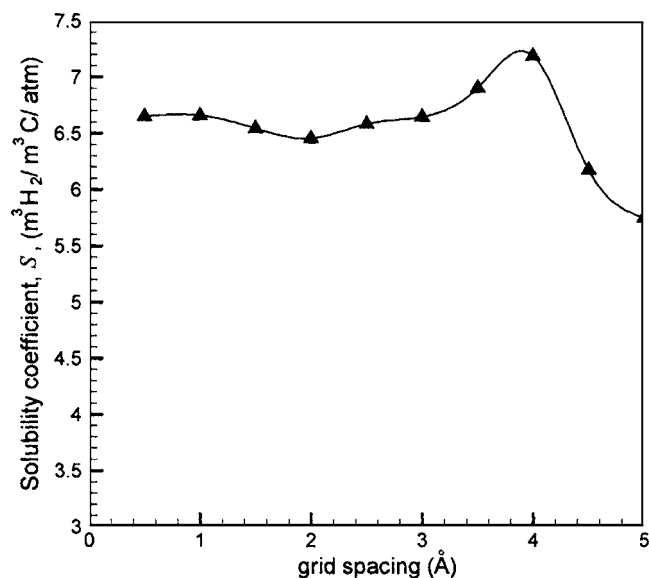


FIG. 4. Dependence of simulation results of solubility coefficient on grid spacing used in the simulations.

illustrates the concept of periodic boundary conditions used for single nanotube simulations. The shaded box represents a simulation cell containing a single-walled nanotube, while the surrounding boxes are exact replica's of this nanotube. This arrangement is imagined to fill the entire space. As a result, carbon atoms in the shaded box are not affected by any surface interactions.

In Fig. 2, R is the cutoff radius that is applied when calculating the potential between a carbon atom and a hydrogen test molecule. The energy calculation only takes into consideration those atoms that fall within the sphere spanned by the cutoff radius and ignores those that fall outside of this sphere. The cutoff radius is one of the important simulation parameters, similar to the iteration number and grid spacing described earlier.

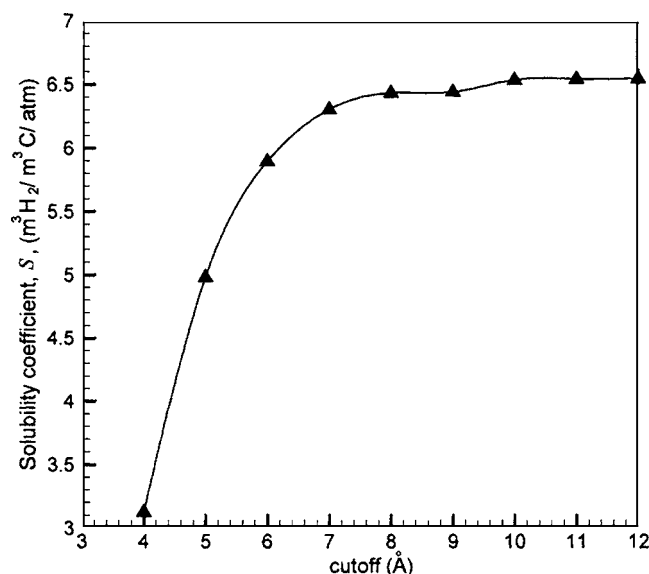


FIG. 5. Dependence of simulation results of solubility coefficient on cutoff radius used in the simulations.

Langmuir isotherm model and adsorption constant

When a gas is in contact with a solid there is an equilibrium established between the molecules in the gas phase and the adsorbed species bound to the surface of the solid. The load factor (coverage of the adsorbed gas on the solid surface), θ , at a fixed temperature is described by the Langmuir isotherm model²² as

$$\theta = \frac{q^*}{q_{\text{sat}}} = \frac{KP}{1 + KP}, \quad (8)$$

where q^* is the number of adsorbed gas molecules, q_{sat} is the number of saturated gas molecules, K is the adsorption constant defined as the ratio of the rate of adsorption to desorption, and P is the pressure. The number of adsorbed gas molecules at a given temperature and pressure can thus be calculated from

$$q^* = q_{\text{sat}} \frac{KP}{1 + KP}. \quad (9)$$

The volumetric hydrogen adsorption in nanotubes, c , can be derived from Eq. (9),

$$c = \frac{\frac{q^* \times 22.4}{Na}}{V} = \frac{\frac{22.4}{Na} q_{\text{sat}}}{V} \times \frac{KP}{1 + KP}, \quad (10)$$

where Na is the Avogadro's constant, V is the volume of nanotubes, and

$$\frac{\frac{22.4}{Na} q_{\text{sat}} K}{V} \quad \text{is the solubility coefficient, } S,$$

obtained from Eq. (2). The volumetric hydrogen adsorption in nanotubes can also be predicted by the Langmuir adsorption model in the form

$$c = \frac{SP}{1 + KP}. \quad (11)$$

Combining Eqs. (10) and (11) to solve for the adsorption constant, K , we have

$$K = \frac{S}{\frac{\frac{22.4}{Na} q_{\text{sat}}}{V}} = \frac{S \times V \times Na}{22.4 q_{\text{sat}}}. \quad (12)$$

The saturation content of hydrogen in carbon nanotubes, q_{sat} , can be estimated using a procedure described as follows. A hydrogen test molecule is randomly inserted into the unoccupied grids of the nanotubes and the energies at each position are calculated. The position with the lowest energy is where the first hydrogen molecule is inserted. The insertion position for additional hydrogen molecules is searched using the same procedure except that now the system includes previously inserted hydrogen molecules. This procedure repeats until no hydrogen molecules can be inserted (the energy change caused by hydrogen insertion is positive) or there are no unoccupied grid points left for insertion. The total number of the inserted hydrogen molecules, q_{sat} , can be used in Eq. (12) to calculate the adsorption constant, K . The

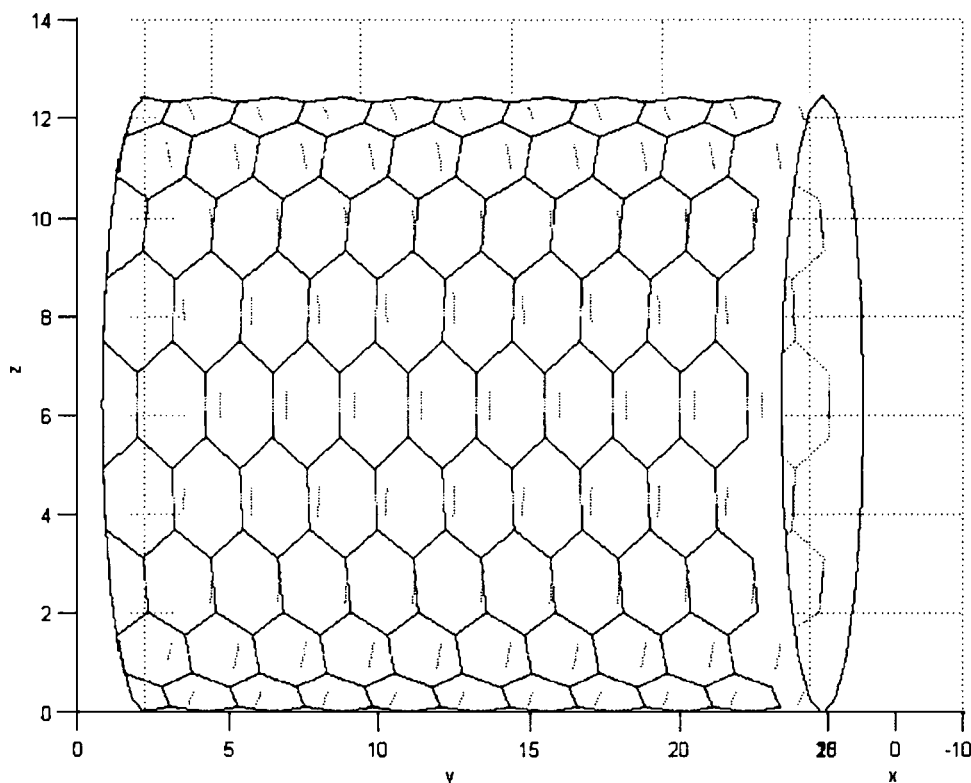


FIG. 6. Three-dimensional view of a single-walled (10,10) armchair carbon nanotube.

values of K and S can then be used to predict the hydrogen adsorption isotherm using the Langmuir adsorption model in Eq. (11).

RESULTS AND DISCUSSIONS

Simulation parameters

The effects of iteration number, grid spacing, and cutoff radius on simulation results of hydrogen adsorption are studied by simulations of a (10,10) armchair single-walled nanotube. As stated in an earlier section, an optimal iteration number can lead to a higher accuracy of calculation of the ensemble average. In order to find the optimal iteration number, three independent runs were performed. The simulated hydrogen solubility coefficient, S , calculated from Eqs. (1) and (2) using different iteration numbers as the ensemble average is shown in Fig. 3. As shown, the simulation results on S are significantly different for iteration numbers smaller than 2500 and the results are not repeatable for three runs. The solubility coefficients for all runs converge at about 10 000 iterations.

The dependence of solubility coefficient on grid spacing is studied and the result is shown in Fig. 4. As shown, the values of the simulated solubility coefficients fluctuate when the grid spacing used for the Monte Carlo simulations is higher than 3 Å. Grid spacing from 1 to 3 Å will yield acceptable results.

As mentioned previously, the cutoff radius is used to reduce the amount of computation when calculating the total energy of a system. Its effect on hydrogen adsorption in a single-walled nanotube is shown in Fig. 5, which suggests that the simulation results on solubility coefficient are no longer sensitive to the cutoff radius when its value is larger than 8 Å. The results presented in the rest of this paper are obtained using an iteration number of 10 000, a grid spacing of 2 Å, and a cutoff radius of 8 Å.

Hydrogen adsorption in a single nanotube

A (10,10) armchair single-walled nanotube containing 400 carbon atoms is constructed as shown in Fig. 6. The bond length between carbon atoms is 1.4 Å. The hydrogen solubility coefficient, S , obtained from Widom's test particle insertion method is $6.5 \text{ m}^3 \text{ H}_2/\text{m}^3/\text{atm}$ at 298 K, and the hydrogen adsorption constant, K , is calculated from Eq. (12) to be 0.011. The volume of the nanotube, V , used in Eq. (12) is 9669 Å^3 . Substituting the values of S and K into Eq. (11), the hydrogen adsorption in unit of volumetric density ($\text{kg H}_2/\text{m}^3 \text{ C}$) as a function of pressure is produced as shown in Fig. 7(a), and the plot of hydrogen gravimetric density ($\text{kg H}_2/\text{kg C}$) versus pressure is shown in Fig. 7(b). Figures 7(a) and 7(b) include results obtained from two slightly different sets of force field parameters: The solid curves represent the solution obtained using the CVFF force field and the dashed lines represent those from a set of parameters used in Refs. 18–20. As is expected, there are slight differences in the results, but not enough to warrant the selection of one over another. The results in Figs. 7(a) and 7(b) show that the hydrogen adsorption rate increases with the pressure following the relationship predicted by the Langmuir adsorption

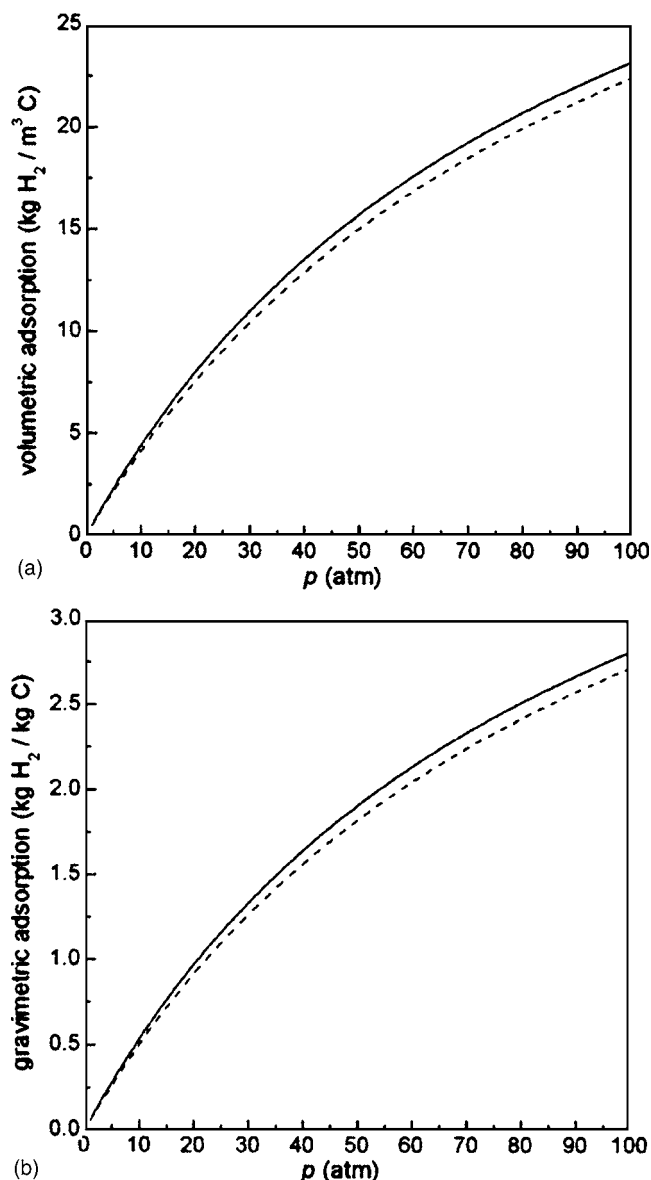


FIG. 7. Volumetric (a) and gravimetric (b) hydrogen adsorption isotherms in a single-walled nanotube at 298 K. Solid lines: results obtained using the CVFF force field parameters; dashed lines: results obtained using a set of force field parameters from Refs. 18–20.

model. The values of solubility coefficient, S , and adsorption constant, K , determine the shape of the isotherm curves. At 100 atm and room temperature, the volumetric hydrogen adsorption was predicted from Fig. 7(a) to be $23.2 \text{ kg H}_2/\text{m}^3$, lower than the DOE target of $62 \text{ kg H}_2/\text{m}^3$.³²

In Widom's test particle insertion method, the potential energy change caused by inserting a hydrogen molecule at a random position, Ψ , can be significantly different depending on the insertion position. Since large Ψ 's have no or little contribution to the canonical average of the interaction energy in Eq. (1), the insertion positions corresponding to these Ψ 's are not acceptable for hydrogen adsorption. The positions in a single nanotube where a hydrogen insertion produces acceptable potential change are shown in Fig. 8. As shown, hydrogen molecules are more likely to be adsorbed at the external surface of the nanotube than inside the nanotube. Therefore, increasing the surface areas outside the nanotubes

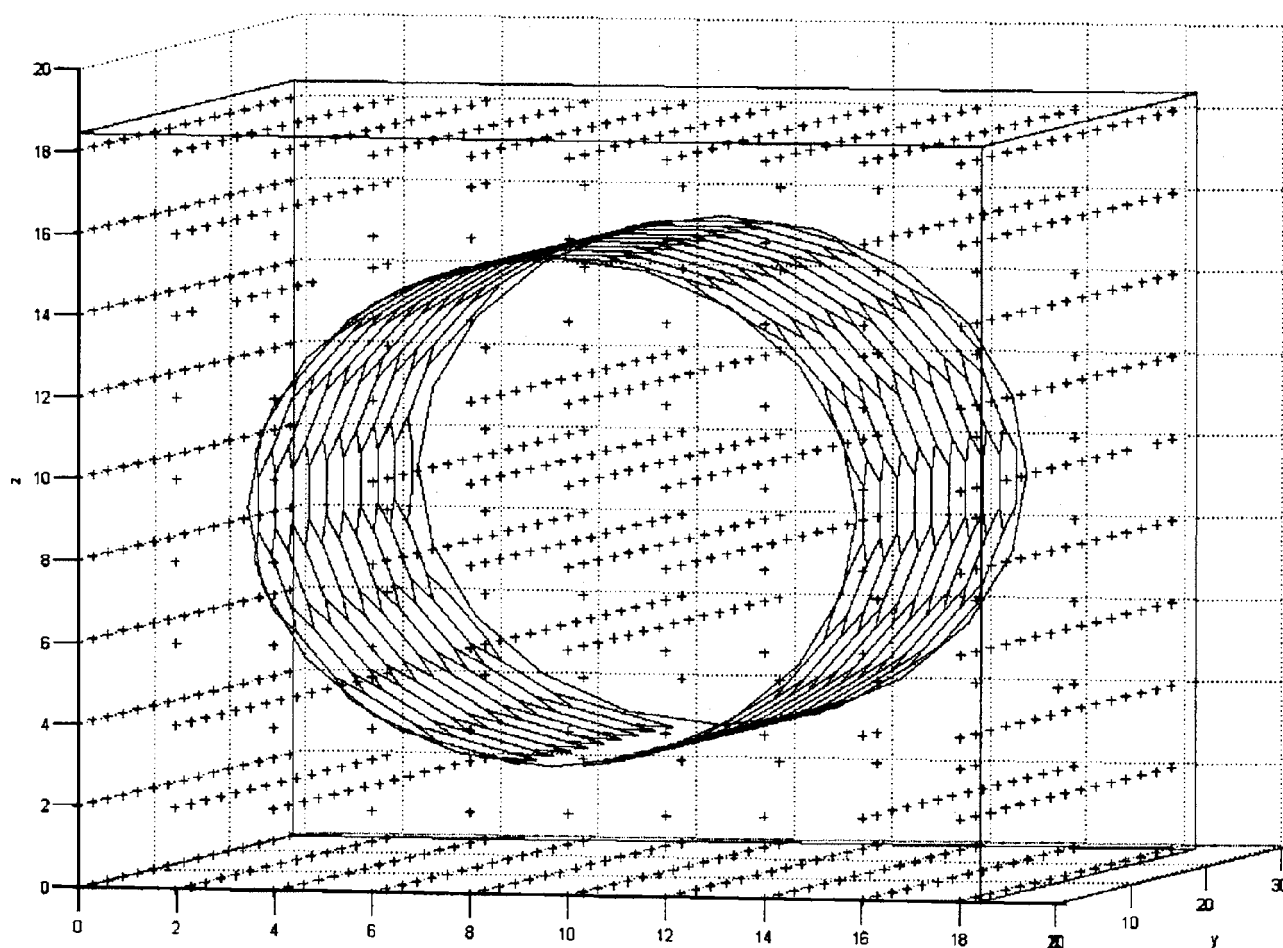


FIG. 8. Schematic view of hydrogen adsorption positions in a single SWNT. The + denotes the position for possible insertion of a hydrogen molecule of which the insertion leads to lower energy of the system.

available to hydrogen may increase the total amount of hydrogen adsorption. One approach to increase space available to hydrogen molecules is to change the configurations and intertube distances of nanotube bundles.

Simulation of hydrogen adsorption in SWNT bundles

Two arrangements of SWNT bundles as shown in Figs. 9(a) and 9(b) were studied. The single nanotubes in the bundles are the same in diameter and length as the single nanotube studied in the previous section. The van der Waals gap, d , is the distance between two single nanotubes as indicated in Fig. 9(a). The influence of intertube distance on hydrogen adsorption was studied for a nanotube bundle of nine single (10,10) armchair SWNTs arranged in the rectangular configuration. Four different intertube distances were used in the simulations; the temperature used in the simulations is 298 K.

The results on adsorption isotherms are plotted in Figs. 10(a) and 10(b). As shown in Fig. 10(a), the volumetric hydrogen adsorption (in units of $\text{kg H}_2/\text{m}^3 \text{C}$) decreases significantly with increasing intertube distance of SWNT bundles. It suggests that increasing the intertube distance of nanotube bundles increases the total volume of carbon nanotubes but the increase of hydrogen adsorption (in unit of kg H_2) is not in proportion. As a result the volumetric hydrogen adsorption

is decreased for sparsely distributed nanotube bundles. However, a larger intertube distance is positive for the hydrogen gravimetric adsorption (in unit of $\text{kg H}_2/\text{kg C}$). Since the total weights of the nanotubes are unchanged in all cases and the increasing intertube distances allow more hydrogen adsorption to take place on the external surface of the nanotubes,⁵ the values of gravimetric hydrogen adsorption are higher for SWNT bundles of large intertube distance. Our simulation results suggest that increasing the intertube distance of nanotube bundles may enhance the amount of hydrogen adsorption however has negative impact on the volumetric density of hydrogen adsorption.

The hydrogen adsorption in SWNT bundles of two dif-

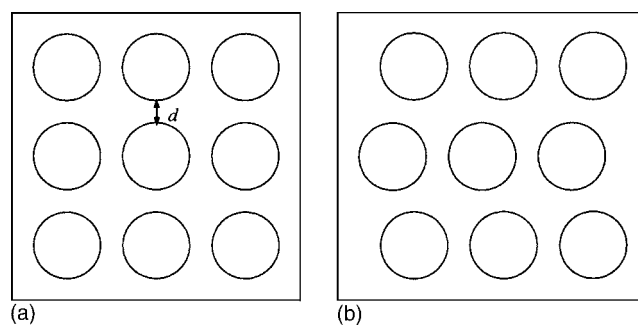
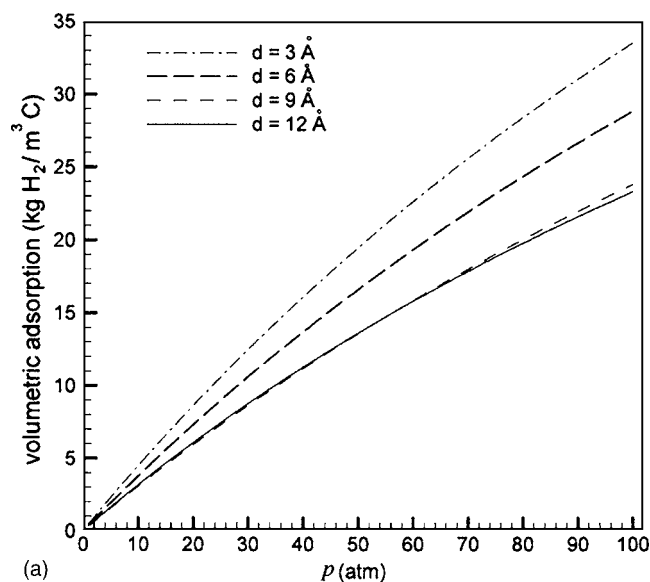
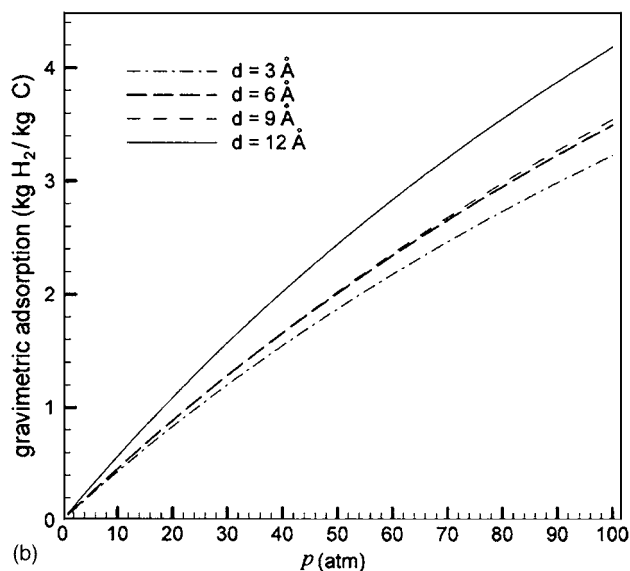


FIG. 9. Rectangular (a) and triangular (b) configurations of SWNT bundles.



(a)



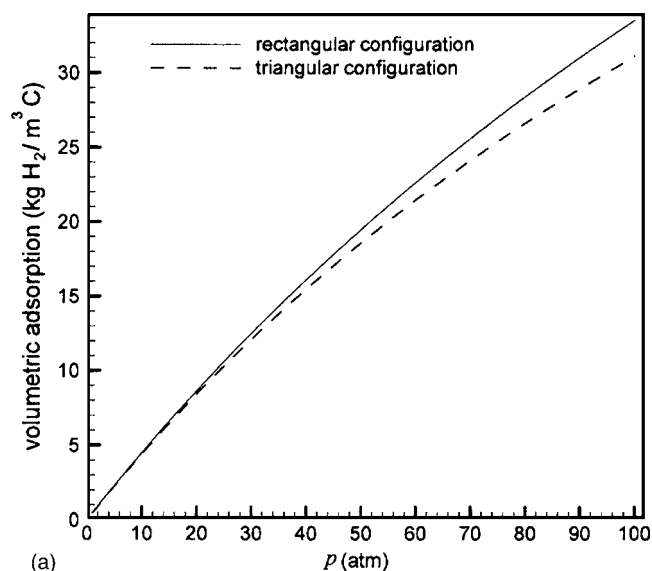
(b)

FIG. 10. Volumetric (a) and gravimetric (b) hydrogen adsorption isotherms in rectangular configuration of SWNT bundles with various values of intertube distance, d .

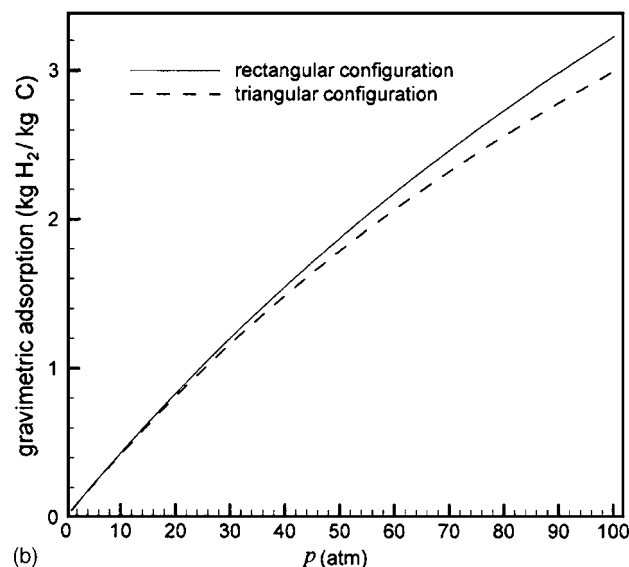
ferent arrangements is compared in Fig. 11 using a intertube distance of 6 Å and a temperature of 298 K. Results show that both volumetric and gravimetric hydrogen adsorption in the rectangular nanotube arrangement is higher than those in the triangular arrangement. It may be attributed to more available intertube space for hydrogen adsorption in the rectangular configuration of nanotube bundles. This result is in good agreement with the observations of Wang *et al.*⁵ who suggest that rectangular arrangement of nanotubes provides higher capacity for hydrogen adsorption.

Simulation of hydrogen adsorption in alkali-doped SWNTs

Alkali-doped carbon nanotubes (CNTs) were first obtained by solid-state reactions between carbon nanotubes and alkali-containing carbonates or nitrates.¹² The ratio of Li/C and K/C of the alkali-doped CNTs was about 1/15 as measured by x-ray photoelectron spectroscopy.¹² Using the same



(a)



(b)

FIG. 11. Volumetric (a) and gravimetric (b) hydrogen adsorption isotherms in rectangular (solid lines) and triangular (broken lines) configurations of SWNT bundles.

alkali/carbon ratio in our simulations, 27 Li⁺ or K⁺ ions were inserted into the single nanotubes, and 240 alkali dopants were used to replace the carbon atoms in the SWNT bundles.

The insertion of alkali dopants can generate many possible configurations of the nanotubes. A Monte Carlo simulation was used to search for the alkali-doped nanotube configurations to be used in Widom's test particle insertion simulations of hydrogen adsorption. The first dopant molecule is inserted at a random position. Subsequently, a number of carbon atoms (27 for a single nanotube, and 240 for SWNT bundle) in a nanotube are replaced by dopant molecules at positions where the replacement will lead to the minimal energy increase among all possible positions. This procedure was repeated for an iteration number of 10 000 and only the ion-doped configurations more stable than the original configuration were used for Widom's test particle insertion simulations of hydrogen solubility.

Widom's test particle insertion simulations were per-

TABLE III. Simulation results of hydrogen adsorption.

SWNT bundles	Solubility coefficient, S (cm ³ /cm ³ /atm)	Adsorption constant, K	Hydrogen adsorption (kg/m ³ C) at 100 atm
Lithium-doped	7.59	0.0055	43.71
Potassium-doped	6.64	0.0044	41.05
No dopants	5.17	0.0038	33.50

formed on lithium- and potassium-doped nanotube bundles and the results on hydrogen solubility and adsorption constant are summarized and compared with the nondoped nanotube bundles in Table III. As shown in Table III, the hydrogen adsorption in lithium- and potassium-doped nanotubes at ambient temperature and 100 atm are 3.95 wt% and

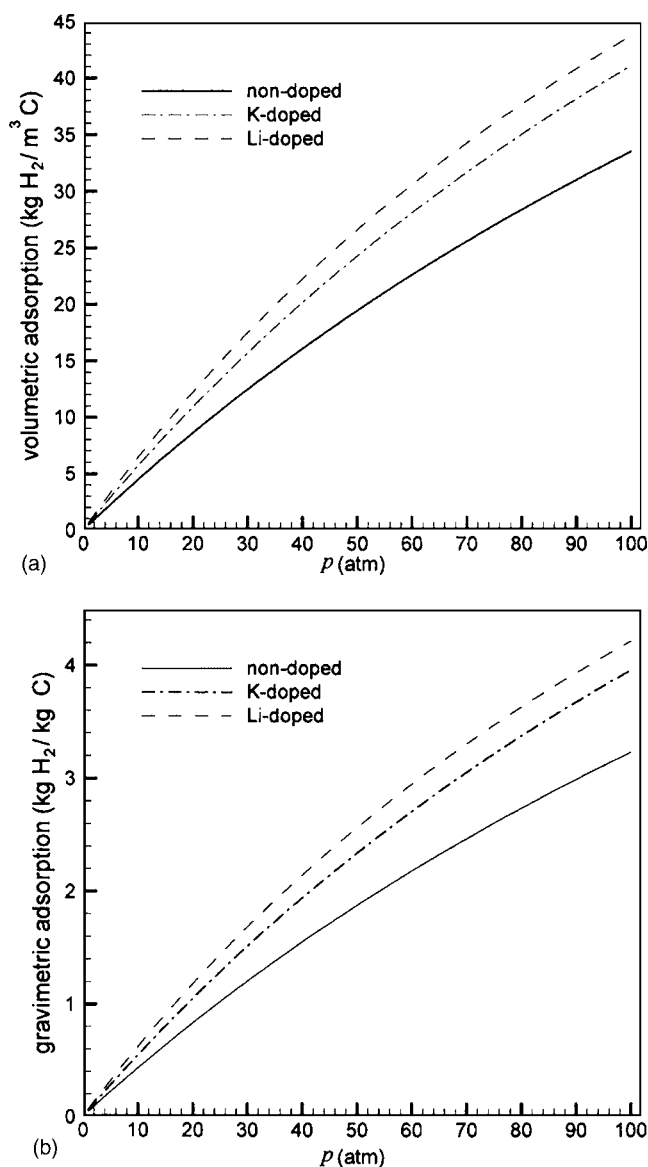


FIG. 12. Volumetric (a) and gravimetric (b) hydrogen adsorption isotherms in nondoped and alkali-doped SWNT bundles. The isotherms were produced using values of solubility coefficient, S , and adsorption constant, K obtained by Widom's test particle insertion and Monte Carlo simulations using a rectangular configuration and an intertube distance of 6 Å.

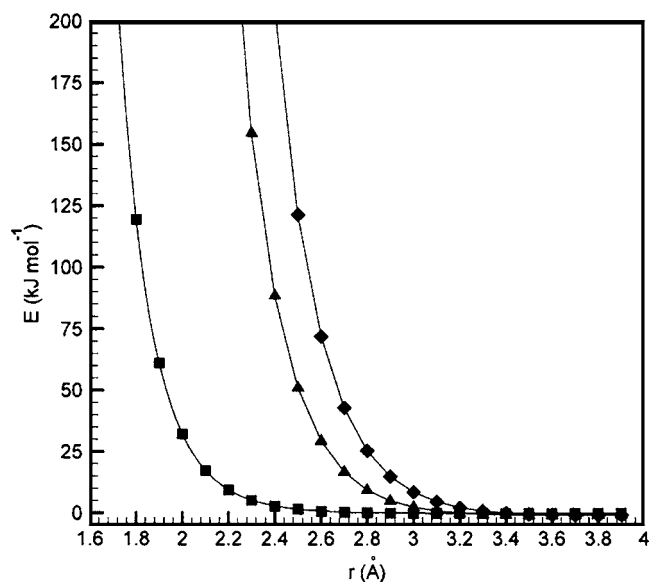


FIG. 13. The Lennard-Jones potential energies as a function of distance between atoms carbon-hydrogen (■), lithium ion-hydrogen (▲), and potassium ion-hydrogen (◆).

4.21 wt%, respectively, higher than the 3.23 wt% hydrogen uptake in SWNTs without doping. Chen *et al.*¹² reported a much higher H₂ uptake density for Li-doped and K-doped MWNTs. Similar studies of alkali-doped multiwall nanotubes by Yang¹³ and Pinkerton *et al.*¹⁴ however, show that the H₂ uptake can only reach 3 wt%. Our results seem to support the conclusions of Yang and Pinkerton *et al.*

The hydrogen adsorption isotherms obtained from the dual model using values of S and K given in Table III, for alkali-doped and nondoped SWNTs are presented in Figs. 12(a) and 12(b). As shown, the increased solubility coefficient and adsorption constant result in higher hydrogen adsorption rates for alkali-doped nanotubes at pressures ranged from 1 to 100 atm.

To investigate the molecular basis of the effect of alkali doping on hydrogen adsorption, the interactions between the H-C pair, as a function of distance, are compared with the interactions between H-Li⁺ and H-K⁺ atom pairs using the Lennard-Jones parameters given in Table I. The potential profiles generated from the Lennard-Jones model in Eq. (2) are shown in Fig. 13. All interaction plots in Fig. 13 indicate a repulsive potential energy at atom distances from 0 to 2 Å. In addition, the repulsion between H and Li⁺ at distances closer than 2 Å is higher than the energy calculated for the H-C pair. This stronger repulsion in H and Li⁺ may lead to more hydrogen molecule insertions at the farther external surface of the nanotubes as shown in Fig. 14. Increased hydrogen adsorption outside the nanotube surface decreases the excess chemical potential and therefore increases the hydrogen solubility coefficient, S . However, the strong repulsion introduced by Li⁺ also decreases the saturation content of hydrogen molecules in the nanotubes, q_{sat} , as introduced in a previous section and therefore yields a higher adsorption constant, K , as indicated in Eq. (10). Therefore, the increased hydrogen solubility coefficient of the alkali-doped nanotubes is accompanied by a larger adsorption constant. Both

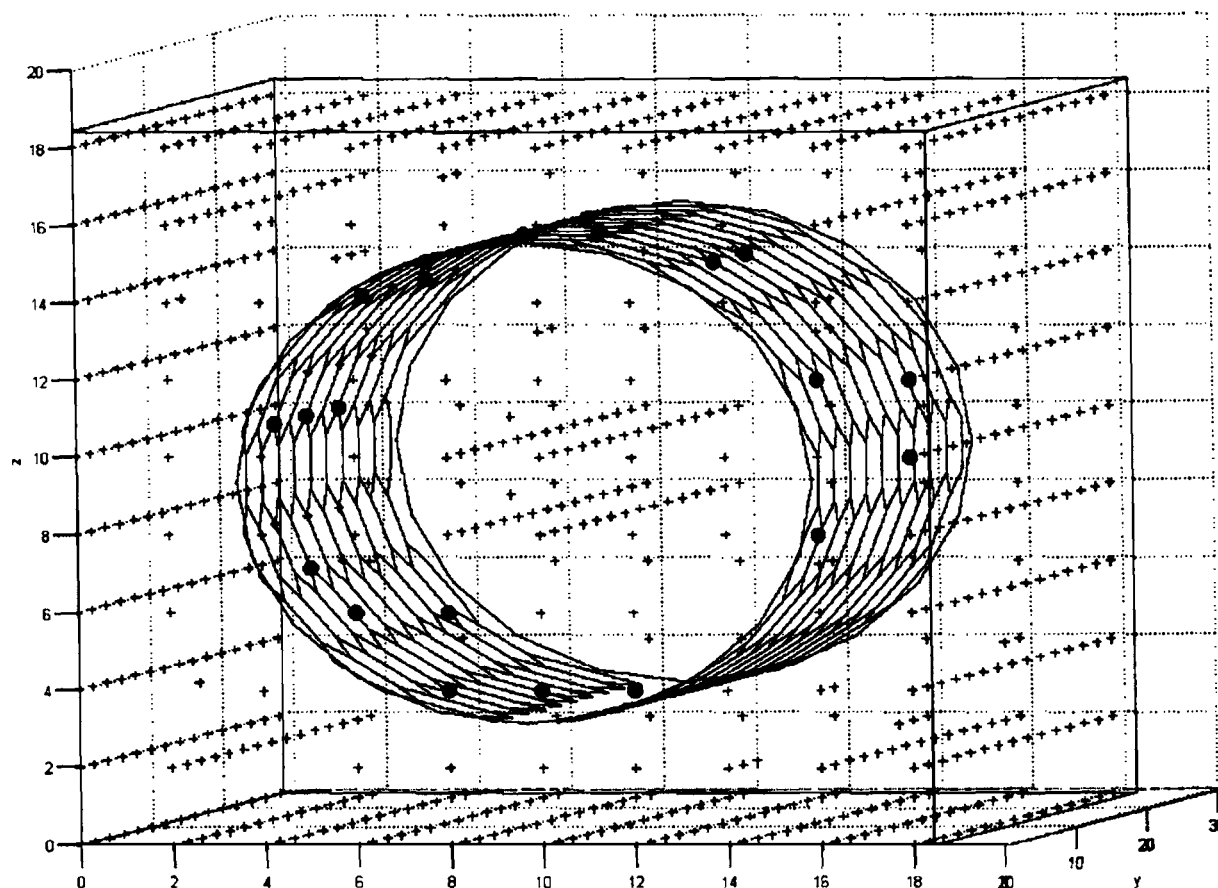


FIG. 14. Schematic view of hydrogen adsorption positions in a lithium-doped single SWNT. The ● symbol indicates the position of lithium dopants, and the + symbol denotes the position for possible insertion of a hydrogen molecule of which the insertion leads to lower energy of the system.

changes of solubility coefficient and adsorption constant contribute to the shape of hydrogen isotherms and the hydrogen adsorption capacity of nanotubes at high pressures. Studies on optimizing the contribution of solubility coefficient and adsorption constant by selecting dopants will be introduced in a follow-up communication with a goal of improving the capacity of nanotube for hydrogen adsorption.

CONCLUSIONS

A Monte Carlo approach using Widom's test particle insertion method was presented in this study to calculate hydrogen storage density of SWNTs. The solubility coefficients (S) and the adsorption equilibrium constants (K) in single-walled (10,10) armchair carbon nanotubes were calculated and used to predict the Langmuir isotherms for hydrogen absorption. The results for single nanotubes, and nanotube bundles with various configurations and alkali dopants are in reasonable agreement with the experimental data obtained at 100 atm and room temperature. The simulations of nanotube bundle configurations and alkali-doped nanotube bundles suggest that both increasing internanotube gap size and introducing alkali dopants can enhance the hydrogen adsorption at external surfaces of nanotubes. While a higher intertube distance has positive effects on gravimetric adsorption densities, it may cause a decrease in the hydrogen volumetric adsorption densities.

ACKNOWLEDGMENTS

The work in this study was partially supported by the Indiana 21st Century Research Fund. We appreciate the discussions on the hydrogen quadrupole moment with Dr. Dykstra of the Department of Chemistry at Indiana University–Purdue University at Indianapolis.

- ¹S. Iijama, *Nature (London)* **354**, 56 (1991).
- ²S. Iijama and T. Ichihashi, *Nature (London)* **363**, 603 (1993).
- ³D. S. Bethune, C. H. Liang, M. S. de Vries, G. Gorman, R. Savoy, J. Vasquez, and R. Beyers, *Nature (London)* **363**, 605 (1993).
- ⁴S. Amelinckx, X. B. Zhang, D. Bernaerts, X. F. Zhang, V. Ivanov, and J. B. Nagy, *Science* **265**, 635 (1994).
- ⁵Q. Wang and J. K. Johnson, *J. Chem. Phys.* **110**, 577 (1999).
- ⁶M. R. Pederson and J. Q. Broughton, *Phys. Rev. Lett.* **69**, 2689 (1992).
- ⁷K. F. Schmidt, *Sci. News (Washington, D. C.)* **143**, 279 (1993).
- ⁸A. C. Dillon, K. M. Jones, T. A. Bekkedahl, C. H. Kiang, D. S. Bethune, and M. J. Heben, *Nature (London)* **386**, 377 (1997).
- ⁹Y. Ye, C. C. Ahn, C. Witham, B. Fultz, J. Liu, A. G. Rinzler, D. Colbert, K. A. Smith, and R. E. Smalley, *Appl. Phys. Lett.* **74**, 2307 (1999).
- ¹⁰C. Liu, Y. Y. Fan, M. Liu, H. T. Cong, and H. M. Cheng, *Science* **286**, 1127 (1999).
- ¹¹H. B. Wu, P. Chen, J. Lin, and K. L. Tan, *Int. J. Hydrogen Energy* **25**, 261 (2000).
- ¹²P. Chen, X. Wu, J. Lin, and K. L. Tan, *Science* **285**, 91 (1999).
- ¹³R. T. Yang, *Carbon* **38**, 623 (2000).
- ¹⁴F. E. Pinkerton, B. G. Wicke, C. H. Olk, G. G. Tibbetts, G. P. Meisner, M. S. Meyer, and J. F. Herbst, *J. Phys. Chem. B* **104**, 9460 (2000).
- ¹⁵Q. Wang and J. K. Johnson, *J. Phys. Chem. B* **103**, 4809 (1999).
- ¹⁶V. V. Simonyan, J. K. Johnson, A. Kuznetsova, and J. T. Yates, *J. Phys. Chem.* **114**, 4180 (2001).
- ¹⁷M. Repzka, P. Lamp, and M. A. Cassa Lillo, *J. Phys. Chem. B* **102**,

- 10894 (1998).
- ¹⁸F. Darkrim and D. Levesque, *J. Chem. Phys.* **109**, 4981 (1998).
- ¹⁹F. Darkrim and D. Levesque, *J. Phys. Chem. B* **104**, 6773 (2000).
- ²⁰F. Darkrim, P. Malbrunot, and G. P. Tartaglia, *Int. J. Hydrogen Energy* **27**, 193 (2002).
- ²¹B. Widom, *J. Chem. Phys.* **39**, 2808 (1963).
- ²²I. Langmuir, *J. Am. Chem. Soc.* **38**, 2221 (1916).
- ²³J. R. Errington, G. C. Boulougouris, I. G. Economou, A. Z. Panagiotopoulos, and D. N. Theodorou, *J. Phys. Chem. B* **102**, 8865 (1998).
- ²⁴J. K. Shah and E. J. Maginn, *Fluid Phase Equilib.* **222–223**, 195 (2004).
- ²⁵A. M. A. Dias, R. P. Bonifacio, I. M. Marrucho, A. A. H. Padua, and M. F. C. Gomes, *Phys. Chem. Chem. Phys.* **5**, 543 (2003).
- ²⁶D. A. Zazueta, D. Curco, C. Aleman, and S. Munoz-Guerra, *J. Polym. Sci., Part B: Polym. Phys.* **41**, 2928 (2003).
- ²⁷D. Zanuy, C. Aleman, and S. Munoz-Guerra, *J. Polym. Sci., Part B: Polym. Phys.* **40**, 2037 (2002).
- ²⁸A. T. Hagler, E. Huler, and S. Lifson, *J. Am. Chem. Soc.* **96**, 5319 (1974).
- ²⁹H. Dodziuk and G. Dolgonos, *Chem. Phys. Lett.* **356**, 79 (2002).
- ³⁰R. G. Cracknell, *Mol. Phys.* **100**, 2079 (2002).
- ³¹M. Carmichael, K. Chenoweth, and C. E. Dykstra, *J. Phys. Chem. A* **108**, 3143 (2004).
- ³²A. C. Dillon and M. J. Heben, *Appl. Phys. A* **72**, 133 (2001).